GA–A23428

IMPROVEMENT OF CORE BARRIERS WITH ECH AND COUNTER-NBI IN DIII–D

by
C.M. GREENFIELD, K.H. BURRELL, T.A. CASPER, J.C. DeBOO, E.J. DOYLE,
P. GOHIL, R.J. GROEBNER, J.E. KINSEY, J. LOHR, M. MAKOWSKI, G.R. McKEE,
M. MURAKAMI, R.I. PINSKER, R. PRATER, C.L. RETTIG, G.M. STAEBLER,
B.W. STALLARD, E.J. SYNAKOWSKI, D.M. THOMAS,
R.E. WALTZ AND THE DIII–D TEAM

JULY 2000

DISCLAIMER

IMPROVEMENT OF CORE BARRIERS WITH ECH AND COUNTER-NBI IN DIII–D

by

C.M. GREENFIELD, K.H. BURRELL, T.A. CASPER,* J.C. DeBOO, E.J. DOYLE,[†]
P. GOHIL, R.J. GROEBNER, J.E. KINSEY,[‡] J. LOHR, M. MAKOWSKI,* G.R. McKEE,[◊]
M. MURAKAMI,[§] R.I. PINSKER, R. PRATER, C.L. RETTIG,[†] G.M. STAEBLER,
B.W. STALLARD,* E.J. SYNAKOWSKI,[ƒ] D.M. THOMAS,
R.E. WALTZ AND THE DIII–D TEAM

*Lawrence Livermore National Laboratory, Livermore, California.
[†]University of California, Los Angeles, California.
[‡]Lehigh University, Bethlehem, Pennsylvania.
[◊]University of Wisconsin, Madison, Wisconsin.
[§]Oak Ridge National Laboratory, Oak Ridge, Tennessee.
[ƒ]Princeton Plasma Physics Laboratory, Princeton, New Jersey.

1. INTRODUCTION

Internal transport barriers (ITB), or regions of reduced ion thermal transport, are a common feature in neutral-beam heated tokamaks [1–5]. The effect of the ITB often extends to the particle and angular momentum channels, and less frequently, to electron thermal transport. Recent experiments in DIII–D allow a comparison of ITBs formed with both co–neutral beam injection (co-NBI; beam ions injected parallel to the plasma current) and counter-NBI (injected antiparallel to the plasma current) [1]. Here we manipulate the E×B shear dynamics by reversing the rotation contribution to the E×B shearing rate $\omega_{E \times B}$ while leaving the sign of the pressure gradient term unchanged. Discharges with counter-NBI, where the pressure gradient and toroidal rotation terms of the shearing rate are aligned, exhibit a broader ITB than that obtained with co-NBI. This is consistent with the E×B shear turbulence suppression paradigm [6], since the counter-NBI discharges do not exhibit the zero crossing in the shearing rate seen with co-injection due to competition between these terms.

Although barriers in the ion thermal transport channel can be reproducibly obtained, the behavior of the electron channel is relatively inconsistent [7,8]. In many cases, electron thermal transport is either unchanged or even slightly increased after the onset of the ITB. Recently, demonstrations of strong electron thermal transport barriers have been reported in the presence of localized electron heating [5,9–11]. Such a regime has been produced in DIII–D, when 0.5 MW of 110 GW electron cyclotron heating (ECH) is applied off axis ($\rho \approx 0.3$) in a low current, low density plasma. E×B shear, although important in controlling the long wavelength turbulence usually associated with ion thermal transport, is not expected to be a significant factor in determining the behavior of the electron channel. Dynamic simulations of the formation of the electron ITB indicate that the leading mechanism for transport reduction here is finite pressure gradient (α) stabilization of turbulence.

2. TESTS OF THE E×B SHEAR PARADIGM WITH COUNTER-NBI

ITB formation in DIII–D usually begins by injecting high power co-NBI into a low density plasma during the initial current ramp [12]. The primary role of this preheat phase is to freeze in a q profile with weak or negative central shear (NCS). Barrier formation usually begins during this phase. The profiles steepen and broaden with increased neutral beam power, with the ion thermal diffusivity χ_i reduced to levels at or below neoclassical. Reversing the direction of the plasma current (the neutral beam geometry is fixed) allows counter-NBI operation. Due to poor beam ion confinement at low current and with counter-NBI, a new preheat phase was developed in which ECH is substituted for the NBI. Direct effects of the ECH are discussed below. This scenario was successful in producing the desired NCS target q profile, after which the addition of high power neutral beams resulted in formation of the internal transport barrier.

Comparison of profiles from similar co-and counter-NBI discharges is shown in Fig. 1. These discharges have similar absorbed NBI power, plasma energy and core q profiles, but the central temperatures and toroidal rotation velocity are considerably higher with co-NBI. However, the barrier regions are broader with counter-NBI.

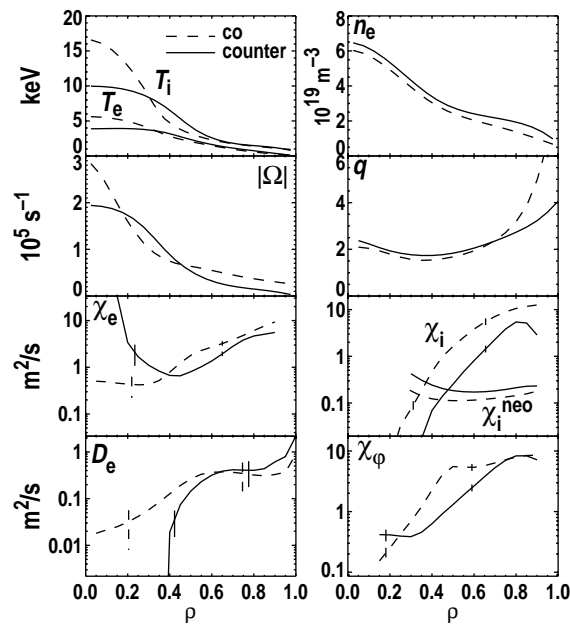Fig. 1. Comparison of profiles from similar discharges (co: 87031 1.82 s, $P_{NBI} = 7.6$ MW (absorbed), $W_{plasma} = 1.2$ MW, counter: 99849 1.17 s, $P_{NB} = 6.5$ MW (absorbed), $W_{plasma} = 0.9$ MW) indicates broader profiles with counter-NBI.

The shearing rate $\omega_{E\times B}$ is calculated from charge exchange recombination measurements of the carbon impurity rotation velocities, density and temperature:

$$\omega_{E\times B} = \frac{(RB_\theta)^2}{B} \frac{\partial}{\partial\psi}\left(\frac{E_r}{RB_\theta}\right) \quad, \tag{1}$$

where

$$E_r = (Z_i e n_i)^{-1}\nabla p_i - v_{\theta i}B_\varphi + v_{\varphi i}B_\theta \quad. \tag{2}$$

i can denote any species; usually the carbon impurity, measured by charge exchange recombination, is used. $\omega_{E\times B}$ can also be written as the sum of pressure gradient and rotation terms:

$$\omega^i_{\nabla p} = \frac{(RB_\theta)^2}{Z_i eB} \frac{\partial}{\partial\psi}\left(\frac{1}{n_i RB_\theta}\nabla p_i\right) \quad, \tag{3}$$

$$\omega^i_{rot} = \frac{(RB_\theta)^2}{B} \frac{\partial}{\partial\psi}\left[\frac{1}{R}\left(v_{\varphi i} - v_{\theta i}\frac{B_\varphi}{B_\theta}\right)\right] \quad. \tag{4}$$

In Fig. 2, the total shearing rate $\omega_{E\times B}$, with its components ω^D_{rot} and $\omega^D_{\nabla p}$ calculated for the deuterium main ions, is shown for the two discharges. $\omega^D_{\nabla p}$ is calculated using the measured impurity temperature (equilibrated with the main ions) and thermal main ion density calculated by TRANSP. We calculate the rotation term by subtracting $\omega^D_{\nabla p}$ from the total shearing rate. The two terms are opposed with co-NBI, and parallel with counter-NBI.

In Fig. 2(c), the absolute values of the two shearing rates are shown together, along with the linear growth rate γ_{max} for low-k (ion temperature gradient; ITG, and/or trapped electron mode; TEM) turbulence calculated by a linear gyrokinetic stability code [13] with non-circular geometry [14] and fully electromagnetic dynamics [15]. The criterion $|\omega_{E\times B}|>\gamma_{max}$ has proven a reliable indicator of stability to these modes both in simulations [16] and in experiments [1,4,6]. Despite the contrasting dynamics of the individual terms, the total shearing rates are of similar magnitude. Both the profile itself, and the region where the shearing rate exceeds the calculated growth rate, are noticeably broader with counter-NBI, indicating an expanded region of stability to ITG and TEM turbulence.

This may indicate removal of a fundamental obstacle toward ITB expansion. If the co-NBI barrier could be forced to expand, the pressure gradient term would increase at the barrier front, thereby *reducing* the total amplitude of the shearing rate and destabilizing turbulence in that region. The same action performed on the counter-NBI discharge would be expected to have the opposite effect, since increasing and/or broadening the pressure profile would now

increase the total amplitude of the shearing rate. Thus, it is expected that further efforts with counter-NBI might result in increased expansion of the barrier region.
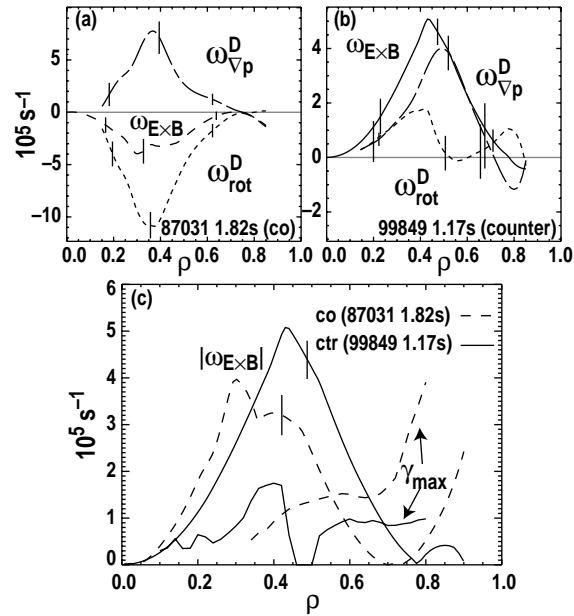

Fig. 2. Shearing rate $\omega_{E \times B}$ and its components ω_{rot}^D and $\omega_{\nabla p}^D$ for the discharges shown in Fig. 1. (a) co-NBI, (b) counter-NBI. (c) Profiles of $|\omega_{E \times B}|$ and the calculated linear growth rate γ_{max} for low-*k* turbulence shown for both discharges.

3. ELECTRON ITB PRODUCED WITH ECH

The ECH preheat employed to prepare the target q profile for ITB formation had additional effects on the plasma. Starting 100–300 ms after the initial breakdown, while the plasma current was 0.4–0.5 MA, the 0.5 MW output from a single 110 GHz gyrotron was injected toward an absorption location of $\rho \approx 0.3$. The antenna phasing was such that the ECH both heated electrons and drove current in the direction opposite to the main plasma current. 0.5 MW of neutral beam power was applied for diagnostic purposes, but most of this power was lost from the plasma due to beam ion orbit losses.

An ITB, most evident in the electron temperature profile, rapidly formed after the activation of ECH (Fig. 3). The electron temperature gradient increased to $\partial T_e / \partial R > 150$ keV/m concentrated within a 3-cm wide region on the outer midplane. T_i remains small due to the small amount of energy entering the ion channel (primarily from electron-ion coupling). Due to ECCD, the q profile has regions of both positive and negative shear in the core. Regions of reduced transport are calculated by TRANSP, with χ_i reduced approximately to neoclassical levels and χ_e reduced essentially to zero. The GKS code [13–15] was again used to calculate the growth rates for drift ballooning modes at the time when the electron temperature gradient was the largest. Since measurements of the poloidal impurity velocity were not available, the shearing rate was calculated as in Eq. (1), but with the v_θ calculated using the NCLASS code. Although neoclassical estimates of v_θ have not proven to be particularly accurate when compared with the measurement, its contribution to $\omega_{E \times B}$ is small here. Figure 4(a) shows a comparison of this estimated $|\omega_{E \times B}|$ with the calculated linear growth rate γ_{max} for low-k modes (in this case, primarily TEM). Here, the criterion $|\omega_{E \times B}| > \gamma_{max}$ is not satisfied.

If the effects of the finite pressure gradient are removed from the calculation by setting the normalized pressure gradient $\alpha = -\mu_0 p'(\psi) \, V'(\psi)(V/4\pi R_0)^{1/2}$ to zero, the growth rate increases significantly. Thus, with sufficiently large α, the low-k turbulence might be stable.

Figure 4(b) shows a comparison of the critical temperature gradient for onset of the ETG mode (high-k) compared to the measured temperature gradient. As has previously been observed [7], the temperature gradient is very close to the critical level throughout most of the ITB region (the larger critical gradient at smaller radii is thought to be a consequence of a numerical instability in the calculation). If the effects of finite α are removed again, the critical gradient is reduced well below the measured level.
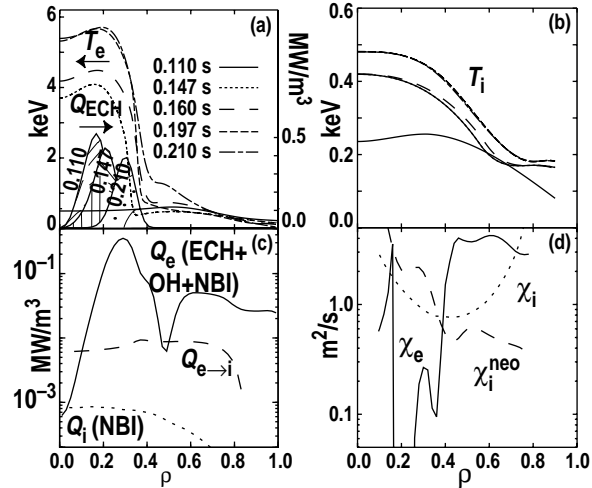
Fig. 3. (a) T_e and ECH heating profiles at several times during the electron ITB evolution, (b) T_i profiles at same times. (c) heating and (d) diffusivity profiles calculated by TRANSP at $t=0.195$ s, the time of the peak ∇T_e. ECH was turned on at $t=0.11$ s. (99696).
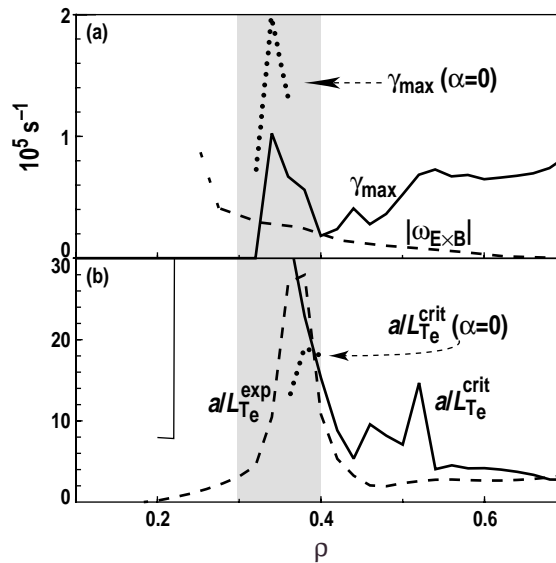

Fig. 4. GKS results: (a) $|\omega_{E\times B}|$ and γ_{max} calculated with finite and zero α, (b) experimental and critical values of normalized ∇T_e, a/L_{Te}. (99696 0.2 s). Shaded region indicates ITB location.

This discharge has been dynamically simulated using the GLF23 model [17]. We use n, q and source profiles from analysis and evolve the T and v_φ profiles beginning prior to ITB

formation. Boundary conditions are enforced by experimental values at $\rho=0.9$. Results of this simulation are shown in Fig. 5. Barriers form in both the temperature profiles and continue evolving until equilibrium. The equilibrium T_e and T_i profiles are remarkably similar to the experimental results. Differences may be accounted for, at least in part, by the fact that resistive interchange mode prevented the experimental profiles from reaching equilibrium. For the simulation to reproduce the experiment, $c_\alpha \equiv \alpha_{used}/\alpha_{calculated}$ was increased to 1.35. With $c_\alpha=1.0$, the simulation did not form a barrier, and at lower values of $c_\alpha<1.0$, a simulation started with a pre-existing ITB could not maintain it.

Both calculations (GKS and GLF23) indicate a strong sensitivity to changes in α which are within experimental uncertainties and predict ITB formation with parameters near those observed in the experiment. This is consistent with earlier calculations indicating α stabilization of turbulence as an important effect [18,19], but this is the first time this has been identified as a likely leading factor in transport reduction in DIII–D.
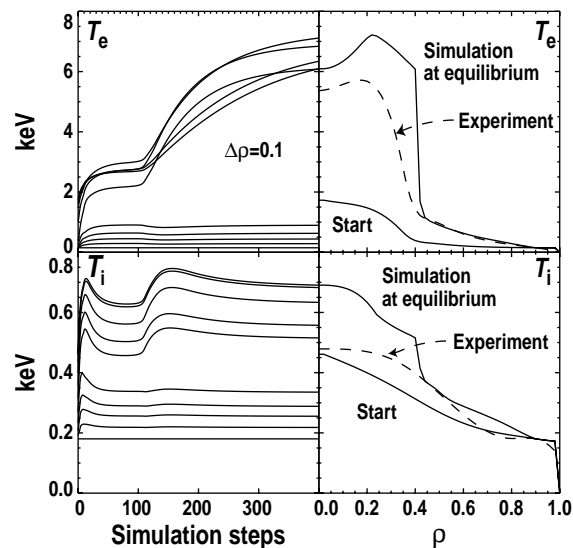

Fig. 5. A dynamic GLF23 simulation indicates formation of an ITB whose equilibrium characteristics are remarkably similar to the measured temperature profiles (99696).

4. SUMMARY

Two classes of ITBs have been examined in recent experiments in DIII–D. The first primarily affects the ion thermal channel. In such cases, E×B shear stabilization of the low-k turbulence associated with the ITG and TEM instabilities is a sufficient condition to obtain the barrier. This appears to be a necessary but not sufficient condition for reducing electron thermal transport. High-k modes, such as electron temperature gradient (ETG) turbulence, are believed to have an impact on transport in the electron, but not in the ion, channel [20]. Due to their smaller spatial scales and larger growth rates, ETG modes are not expected to respond to E×B shear. Another mechanism must be active in order to stabilize these modes and establish an electron ITB. Comparison of electron ITB characteristics with numerical predictions indicates that this role may be played by α stabilization of turbulence.

ACKNOWLEDGEMENTS

REFERENCES

[1] C.M. Greenfield, J.C. DeBoo, T.C. Luce, *et al.*, Phys. Plasmas **7**, 1959 (2000).

[2] H. Shirai, M. Kikuchi, T. Takizuka, *et al.*, Nucl. Fusion **39**, 1723 (1999).

[3] C. Gormezano, Y.F. Baranov, C.D. Challis, *et al.*, Phys. Rev. Lett. **80**, 5544 (1999).

[4] E.J. Synakowski, S.H. Batha, M.A. Beer, *et al.*, Phys. Rev. Lett. **78**, 2972 (1997).

[5] R. C. Wolf, S. Günter, F. Leuterer, *et al.*, Phys. Plasmas **7**, 1839 (2000).

[6] K.H. Burrell, Phys. Plasmas **4**, 1499 (1997).

[7] B.W. Stallard, C.M. Greenfield, G.M. Staebler, *et al.*, Phys. Plasmas **6**, 1978 (1999).

[8] M.C. Zarnstorff, Bull. Am. Phys. Soc. **43**, 1635 (1998).

[9] P. Buratti, E. Barbato, G. Bracco, *et al.*, Phys. Rev. Lett. **82**, 560 (1999).

[10] P. Mantica, private communication (2000).

[11] G.T. Hoang, C. Bourdelle, X. Garbet, *et al.*, Phys. Rev. Lett. **84**, 4593 (2000).

[12] C.L. Rettig, K.H. Burrell, B.W. Stallard, *et al.*, Phys. Plasmas **5**, 1727 (1998).

[13] M. Kotschenreutner, Bull. Am. Phys. Soc. **37**, 1432 (1992).

[14] R.L. Miller, M.S. Chu, J.M. Greene, *et al.*, Phys. Plasmas **5**, 973 (1998).

[15] R.E. Waltz, W. Dorland, private communication (1998).

[16] R.E. Waltz, Phys. Plasmas **5**, 1784 (1998).

[17] R.E. Waltz, G.D. Kerbel, J. Milovich, Phys. Plasmas **1**, 2229 (1994).

[18] M.A. Beer, G.W. Hammett, G. Rewoldt, *et al.*, Phys. Plasmas **4**, 1499 (1997).

[19] R.E. Waltz, G.M. Staebler, W. Dorland, *et al.*, Phys. Plasmas **4**, 2482 (1997).

[20] F. Jenko, W. Dorland, M. Kotschenreuther, B.N. Rogers, Phys. Plasmas **7**, 1904 (2000).